Catalysis Today 148 (2009) 251–259

Contents lists available at ScienceDirect

Catalysis Today

journal homepage: www.elsevier.com/locate/cattod

Rh/Ce-SBA-15: Active and stable catalyst for CO_2 reforming of ethanol to hydrogen

Xusheng Wu, Sibudjing Kawi *

Department of Chemical and Biomolecular Engineering, National University of Singapore, 4 Engineering Drive 4, Singapore 119260, Singapore

ARTICLE INFO

Article history:
Available online 10 September 2009

Keywords:
SBA-15
CO_2 reforming
Ethanol
Cerium
Hydrogen
Syngas
Surface oxygen mobility
Rhodium catalyst

ABSTRACT

CO_2 reforming of ethanol has been investigated for hydrogen production by reacting CO_2, which is a greenhouse gas, with ethanol, which is a renewable energy source, over Rh/Ce-SBA-15 catalysts. A series of Rh/Ce-SBA-15 catalysts have been prepared using Ce-SBA-15 supports with different Ce/Si molar ratio synthesized by direct synthesis method. The catalysts have been characterized by TEM, FESEM, XRD, BET, TPR, TPD and XPS. All samples show high surface area and mesoporous structure at high Ce/Si (= 0–1/5), whereas the mesoporous structure is destroyed at high Ce/Si molar ratio (= 1/1). The catalytic tests show that the Ce/Si molar ratio of the catalysts has significant influence on the hydrogen production rate and product selectivity. The optimal Ce/Si molar ratio for the highest hydrogen production rate is found to be 1/20. The increase of catalytic activity of 1%Rh/Ce-SBA-15 from Ce/Si = 0 to Ce/Si = 1/20 is attributed to the increase of the amount of Ce incorporated into SBA-15 framework, resulting in the enhancement of the mobility of surface oxygen species. The 1%Rh/Ce-SBA-15 (Ce/Si = 1/20) is found to be the most active, selective and stable catalyst for CO_2 reforming of ethanol to syngas or hydrogen.

1. Introduction

Global climate change and greenhouse effect have already been regarded as a long-term international problem faced by every country all over the world. Global warming and greenhouse effect are related to atmospheric CO_2 accumulation [1]. Rising CO_2 level in atmosphere have extensive effects on several aspects, such as the increasing intensities of hurricanes [2], influence of El Nino phenomena [3], reduced calcification of marine plankton [4,5], and deglaciation [6]. Therefore, chemical utilization of CO_2, which is one of the main greenhouse gases, has become a challenging and attractive subject to deal with the above serious issues. CO_2 reforming with methane has become one of most important methods to transform reactants containing CO_2 to valuable chemicals, such as syngas or hydrogen.

CO_2 reforming of ethanol has several advantages. First, ethanol is renewable, biodegradable, easily transportable, less dangerous and less toxic, while methane is non-renewable and highly explosive [7–9]. Second, CO_2 reforming of ethanol is thermodynamically favorable above 318 °C, whereas CO_2 reforming of methane thermodynamically requires reaction temperature over 642 °C [10]. Third, the main reaction of CO_2 reforming of ethanol:

$$C_2H_5OH + CO_2 \rightarrow 3CO + 3H_2 \quad (\Delta H^\circ_{298\,K} = +297\,kJ/mol) \qquad (1)$$

produces syngas with a theoretical CO/H_2 molar ratio = 1 which is suitable for the production of liquid hydrocarbons or oxygenated hydrocarbons [11,12].

However, some side reactions also occur in CO_2 reforming of ethanol, such as: ethanol decomposition (2), dehydration reaction (3) and reverse water gas shift reaction (4) [12,13].

$$C_2H_5OH \rightarrow CH_4 + CO + H_2 \quad (\Delta H^\circ_{298\,K} = +49\,kJ/mol) \qquad (2)$$

$$C_2H_5OH \rightarrow C_2H_4 + H_2O \quad (\Delta H^\circ_{298\,K} = +45\,kJ/mol) \qquad (3)$$

$$CO_2 + H_2 \rightarrow CO + H_2O \quad (\Delta H^\circ_{298\,K} = -39.5\,kJ/mol) \qquad (4)$$

Reaction (1) is kinetically favored at high temperature because it is strongly endothermic, reactions (2) and (3), which are moderately endothermic, are favored at middle reaction temperature range, whereas reaction (4), which is moderately exothermic, is generally suppressed at high temperature. Therefore, in order to produce high hydrogen production rate, high reaction temperature is chosen for CO_2 reforming of ethanol so that reaction (1), which produces hydrogen, can be enhanced and reaction (4), which consumes hydrogen, can be depressed.

Generally, evaluation of catalytic performance is based on activity, selectivity, stability, and deactivation. One of the reasons which cause catalyst deactivation is the formation of coke during CO_2 reforming of ethanol because ethanol could be decomposed to produce coke which caused deactivation at high reaction temperature [13,14]. Coke formation is also generally observed during CO_2 reforming of methane [12]. The related reactions causing carbon deposition over catalysts in CO_2 reforming of

* Corresponding author. Tel.: +65 6516 6312; fax: +65 6779 1936.
E-mail address: chekawis@nus.edu.sg (S. Kawi).

0920-5861/$ – see front matter © 2009 Elsevier B.V. All rights reserved.
doi:10.1016/j.cattod.2009.08.006

ethanol are listed as follows [14–16]:

$$2CO \rightarrow CO_2 + C \quad (\Delta H^{\circ}_{298\,K} = -171\ kJ/mol) \tag{5}$$

$$CH_4 \rightarrow 2H_2 + C \quad (\Delta H^{\circ}_{298\,K} = +75\ kJ/mol) \tag{6}$$

$$C_2H_5OH \rightarrow C + CO + 3H_2 \quad (\Delta H^{\circ}_{298\,K} = +125\ kJ/mol) \tag{7}$$

$$C_2H_4 \rightarrow \text{Polymerization} \rightarrow \text{Coke} \tag{8}$$

Therefore, inhibition of carbon deposition over catalysts is critical to prolong the catalyst life. Carbon deposition significantly depends on the active metals, indicating that different active metals have large difference in coke formation. For example, Ni-based catalysts were reported to easily deactivate due to the formation of coke from the main reactions of CO_2–ethanol reforming and other ethanol reforming reactions [17–23], as well as from the side reaction of ethanol decomposition [24].

However, Rh-based catalysts are known to have high activity, stability and low coke formation in CO_2 reforming of methane and steam reforming of ethanol reactions [25–28]. Rh is the most active metal in steam reforming of ethanol and the order of the activity of metals in steam reforming of ethanol is as follows: Rh > Pd > Ni = Pt [25]. No coke formation was detected over Rh/La_2O_3 catalysts in CO_2 reforming of methane [26]. Besides catalytic activity, Rh is found to be the most stable group VIII metals for CO_2 reforming of methane [27]. Furthermore, Rh has been shown to have excellent conversion and selectivity to syngas at very short contact time in CO_2–methane reforming reactions [28]. Therefore, Rh-based catalysts have been chosen for investigation in this study for CO_2 reforming of ethanol.

Although active Rh metal plays a very important role in catalysis, however catalyst supports also show significant effects on the catalytic performance due to the metal dispersion and metal-support interaction. Therefore, in order not only to improve catalytic performance but also to reduce coke formation, a high-surface-area catalyst support is generally used to disperse metallic particles, which would make the catalyst not only active but also stable due to the low coke formation on highly-dispersed metallic particles. SBA-15, which has a mesoporous structure with high surface area (>500 m^2/g), uniform pore size (tunable from 4.6 nm to 30 nm) and thick wall (around 4 nm) has been chosen in this study as the catalyst support for active Rh metal particle [29–31]. Although SBA-15 is generally not suitable for steam reforming of ethanol as the ordered structures of SBA-15 have been observed to be partially destroyed by the presence of steam in hydrothermal conditions [32,33], however SBA-15 based catalyst is suitable for CO_2 reforming of ethanol as this reaction does not have any water in the reaction system. Furthermore, incorporation of Ce in SBA-15 mesoporous structure has been found to promote the mobility of surface oxygen species over the catalyst surface [33–36] because CeO_2 shows strong oxygen storage ability with $Ce^{4+} \leftrightarrow Ce^{3+}$ redox and oxygen vacancy formation [37].

In this study, catalytic CO_2 reforming of ethanol is investigated for the production of hydrogen/syngas through utilization of CO_2, which is a greenhouse gas, with ethanol, which is a renewable energy source. A series of Rh/Ce-SBA-15 catalysts, with Ce/Si molar ratios ranging from 0 to 1, have been synthesized and tested for this reaction, with the aim of finding the influence of Ce on the activity, selectivity and stability of catalysts.

2. Experimental

2.1. Preparation of catalysts

Ce-SBA-15 catalyst supports were prepared by hydrothermal synthesis method as reported by Zhao et al. and Song et al. [38,39], using TEOS (Aldrich) as the silica source and P123 [(EO)20(PO)70(EO)20, M_{av} = 5800, Aldrich] as the structure-directing agent. The molar composition of Ce-SBA-15 series catalyst supports was $1SiO_2$: (0, 1/40, 1/20, 1/10, 1/5 or 1) CeO_2: 0.017P123: 2.9HCl: 202.6H_2O. Typically, the above mixture was stirred at 40 °C for 1 day followed by crystallization under static condition for 2 days at 100 °C. The white products were washed and recovered by DI water, and then dried overnight in an oven at 60 °C. Subsequent calcination of white products in the air was carried out at 550 °C for 5 h to remove the template.

1 wt%-Rh/Ce-SBA-15 series catalysts were prepared by wet impregnation method. Ce-SBA-15 powder was mixed with $Rh(NO_3)_3$ solution under magnetic stirring at ~95 °C to achieve 1 wt%-Rh/Ce-SBA-15. After stirring, the solution was dried and then calcined in air at 600 °C for 5 h. Rh/Ce-SBA-15 catalyst of 40–60 mesh was used in a fixed bed reactor.

2.2. Characterization of catalysts

XRD (X-ray diffraction) was used to characterize the material structure, crystalline lattice and composition. The XRD patterns was measured using Shimadzu XRD-6000 under 30 mA current and 40 kV voltages, and a continuous scan angle 2θ was selected from 10° to 80°. A divergence slit was inserted between the X-ray and the sample to ensure the interaction of X-ray beam with the sample.

DTA and TGA (Differential thermal analysis and thermogravimetric analysis) were performed by using Shimadzu DTG-50 thermogravimetric analyzer. DTA was used to determine the rate of temperature change of the sample and TGA was used to determine the weight lost of the sample material when it was heated at constant heating rate of 10 °C/min from room temperature to 800 °C.

TEM (Transmission Electron Microscope) images of 1%Rh/Ce-SBA-15 catalysts were collected using JOEL electron microscope (JEOL JEM-2010, equipped with OXFORD INCA EDS analyzer). Typically, one droplet of ultrasonically-dispersed suspension of 1%Rh/Ce-SBA-15 series catalysts in DI water was added to the copper grid on the copper film and the drying was carried out in an oven at 60 °C.

BET (Brunauer–Emmett–Teller, Autosorb-1, Quantachrome) was used to analyze the surface area and pore size of 1%Rh/Ce-SBA-15 series catalysts by nitrogen adsorption and desorption isotherms. The sample was degassed at 100 °C to remove the adsorbed water and impurities before measurement.

XPS (X-ray Photoelectron Spectroscopy) analyses were performed on KRATOS AXIS HIS 165 to investigate the change of valence for cerium and oxygen. Anode HT with a voltage of 15 kV, a current of 10 mA and a pass energy of 80 eV was used. The photoelectron takeoff angle was 90 °C.

H_2–TPD (Hydrogen chemisorption and tempertature-programmed desorption) was performed on ChemBET 3000 (Quantachrome, TPD/TPR system) to obtain Rh dispersion. Typically, 50 mg of catalyst was reduced at 450 °C for 60 min followed by H_2 adsorption at 30 °C for 60 min. The sample was then purged with N_2 gas to remove the physically adsorbed H_2, followed by heating the sample from room temperature to 800 °C under a heating rate of 10 °C/min. H_2 pulse titration experiment was also conducted using the same system. Since 1 ml of H_2 was used in H_2 pulse titration experiment, the total consumption of H_2 in H_2–TPD was obtained by comparing the H_2 peak areas observed in H_2–TPD with that observed in pulse titration experiment. The amount of Rh atoms on the catalyst surface was calculated based on the amount of desorbed H_2, assuming that one hydrogen molecule was adsorbed on two Rh atoms of the catalyst surface [40]. Rh dispersion was then calculated based on the percentage of Rh

atoms on the catalyst surface with respect to the total Rh atoms in the catalysts.

TPR (Temperature-programmed reduction) analysis was performed using ChemBET 3000. In a typical experiment, 50 mg of catalyst loaded in a U-shape quartz tube was degassed with N_2 gas for 1 h at 500 °C. After this heat treatment, 5% H_2/N_2 mixed gas was introduced to system, followed by heating the sample from room temperature to 800 °C under a heating rate of 10 °C/min. Since H_2 pulse titration experiment was also conducted using the same TPR/TPD system using 1 ml of H_2, therefore the total consumption of H_2 required in the TPR measurement can be obtained by comparing the H_2 peak areas observed in TPR with that observed in pulse titration experiment. The amount of H_2 consumption on different Rh catalysts was similarly calculated based on the corresponding H_2 peak areas.

2.3. Reaction system of CO_2 reforming of ethanol

CO_2 reforming of ethanol was conducted in a stainless steel tube reactor (Ø = 6 mm) fitted in a tube furnace and linked to an online gas chromatograph to analyze the molar percentage of each component in the gas product. Depending on the CO_2:ethanol molar ratio, a certain amount of ethanol was pumped using a syringe pump (ISCO Model 100DM) into the vaporizer (maintained at 150 °C) before entering tube reactor. In a typical CO_2 reforming of ethanol reaction, 100 mg of catalyst was loaded into the stainless steel reactor and reduced under a stream of 25% hydrogen/nitrogen mixed gas at 450 °C for 30 min prior to CO_2 reforming of ethanol.

3. Results and discussion

3.1. Effect of active metals over SBA-15 supports on hydrogen production rate for CO_2 reforming of ethanol

Fig. 1 shows the hydrogen production rates, per amount of metal catalyst, of four active metals – Rh, Ni, Co, Pd – supported on SBA-15 supports. The 5%Ni/SBA-15 catalyst shows the poorest activity on the hydrogen production rate among these five SBA-15 supported catalysts. The 1%Rh/SBA-15 catalyst exhibits the highest hydrogen production rate, about ~470% more active than the 5%Rh/SBA-15.

Fig. 2 shows the TGA–DTA curves characterizing the amount of carbon deposited on these five SBA-15 supported metal catalysts after 1 h of CO_2–ethanol reforming reaction. The amount of carbon deposited on the 1%Rh/SBA-15 catalyst is about 1/7, 1/5, 1/4 and 6/5 of the amount of carbon deposited on

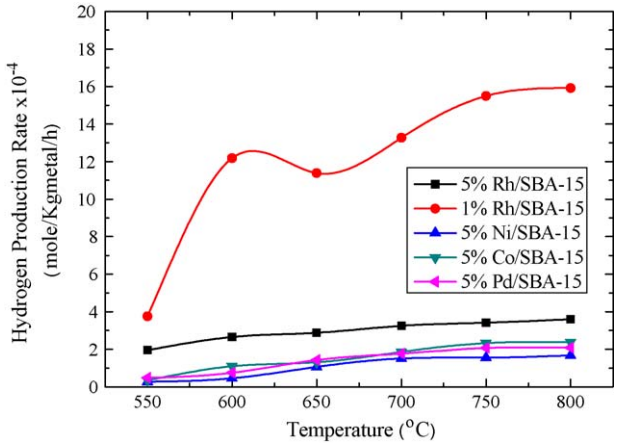

Fig. 1. Effect of active metals over hydrogen production rate over SBA-15 supports (molar ratio of C_2H_5OH/CO_2 = 1:1, GHSV = 15594 h^{-1}).

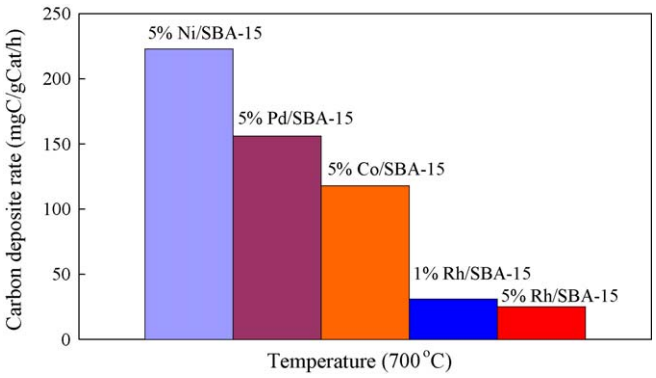

Fig. 2. Carbon deposit over five SBA-15 supported catalysts during 1 h testing by TGA–DTA analysis (molar ratio of C_2H_5OH/CO_2 = 1:1, reaction temperature: 700 °C, GHSV = 15594 h^{-1}).

the 5%Ni/SBA-15, 5%Pd/SBA-15, 5%Co/SBA-15 and 5%Rh/SBA-15 catalysts, respectively. Although the 1%Rh/SBA-15 catalyst has slightly more amount of carbon deposited than the 5%Rh/SBA-15 catalyst, the 1%Rh/SBA-15 catalyst is still the most suitable choice of catalyst among these catalysts for our subsequent studies for CO_2–ethanol reforming as the 1%Rh/SBA-15 catalyst has much less amount of rhodium catalyst than the 5%Rh/SBA-15 catalyst and yet the 1%Rh/SBA-15 catalyst produces the highest hydrogen production rate. Therefore, a series of 1 wt%Rh catalyst supported on SBA-15 with different Ce content has been chosen for further study in order to investigate whether there is any synergetic effect of Ce on improving the catalytic activity and stability of the supported Rh catalytst.

3.2. Morphology of Ce-SBA-15 supports and 1%Rh/Ce-SBA-15

Fig. 3 shows the TEM images of a series of Ce-SBA-15 catalyst supports with Ce/Si molar ratio ranging from 0 to 1. The diameter of the mesopores of Ce-SBA-15 is observed to be around 7 nm and the wall thickness is around 3.5 nm. The TEM images show that the ordered mesoporous structures are kept intact with the increase of the Ce/Si molar ratio from 0 up to 1/5. Above the Ce/Si ratio of 1/5, some of these ordered mesopores start to be destroyed, and at the Ce/Si ratio of 1, most of the mesopores have been destroyed. These TEM results indicate that the Ce-SBA-15 with Ce/Si ratio of 1/20 is the best mesoporous support as it is incorporated with the highest amount of Ce in the mesoporous framework.

Fig. 4 shows the TEM image of the fresh 1%Rh/Ce-SBA-15 catalyst (Ce/Si = 1/20). The size of Rh particles on Ce-SBA-15 (Ce/Si = 1/20) support is found to be around 3–8 nm, which is much smaller than the size of Rh particles of around 50 nm supported on SBA-15 (without cerium) as reported in the literature [41]. Fig. 4 also shows that the ordered mesopores of 1%Rh/Ce-SBA-15 catalyst are still intact even after wet impregnation with Rh precursor followed by high temperature calcination. Mu et al. reported that the high surface area and mesoporosity of Ce-SBA-15 promoted the dispersion of Co_3O_4, which enhanced the catalytic performance for oxidation of benzene due to the synergetic effect between Co and Ce ions [42]. Xu et al. also reported that the strong metal-support interaction between Au and Co oxide over Au/Co-SBA-15 was highly related to the catalytic performance for CO oxidation [43]. Therefore, we believe that there is some interaction between Rh and Ce species which helps to disperse Rh over Rh/Ce-SBA-15 catalysts [42,43].

3.3. XRD patterns of 1%Rh/Ce-SBA-15 based catalysts

Fig. 5 shows the small angle XRD patterns of a series of 1%Rh/Ce-SBA-15 catalysts, with Ce/Si molar ratio ranging from 0 to 1. The

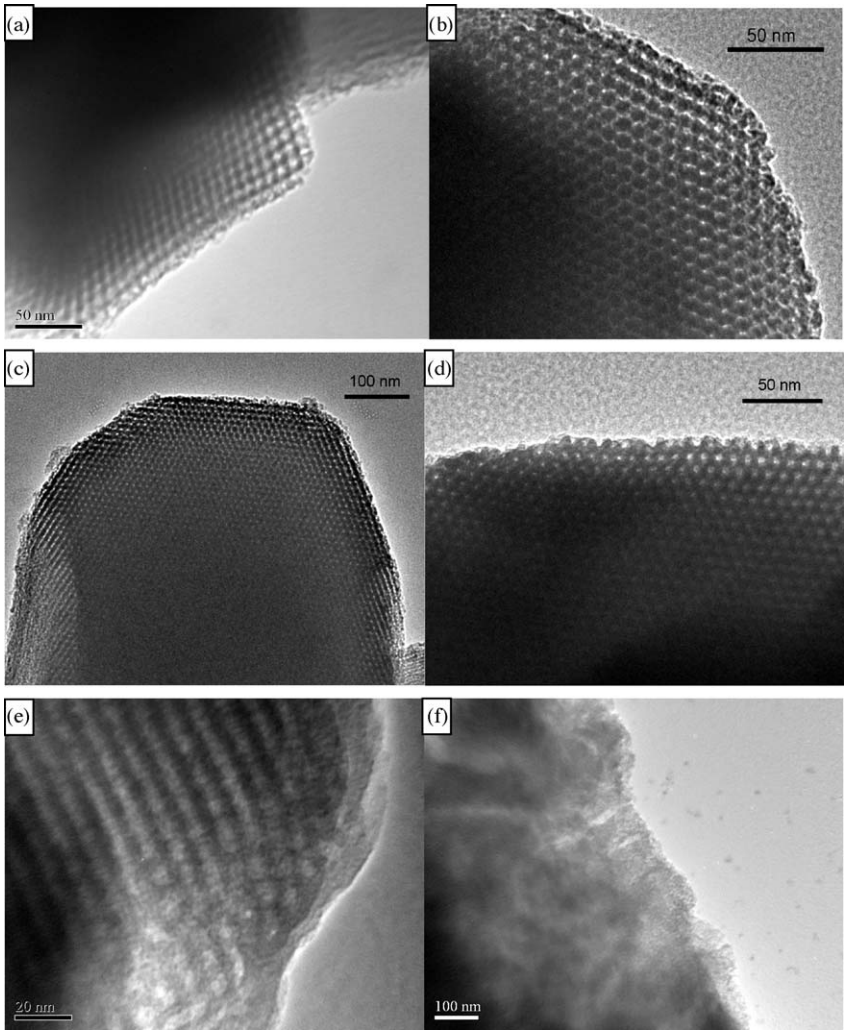

Fig. 3. TEM images of Ce-SBA-15 catalyst supports at different Ce/Si molar ratios, (a) 0, (b) 1/40, (c) 1/20, (d) 1/10, (e) 1/5, (f) 1/1.

characteristic XRD peaks of mesoporous structure with the 2θ values at ~0.7° can be observed over all 1%Rh/Ce-SBA-15 catalysts [42,44,45]. When the Ce/Si molar ratio is increased from 0 to 1/20, the characteristic reflection peaks shifts to lower angle. This XRD result shows that the mesopore diameter has increased, indicating that Ce has been incorporated into the mesoporous framework of SBA-15. However, when the Ce/Si molar ratio is further increased from 1/20 to 1/1, the characteristic XRD reflection peak shifts to higher angle, indicating that the diameter of the mesopores has decreased. Since the TEM results (Fig. 3) has shown that some mesoporous structures could be destroyed at higher Ce content (Ce/Si ratio = 1/1), therefore both the XRD and TEM results show that the destruction of mesoporous structures

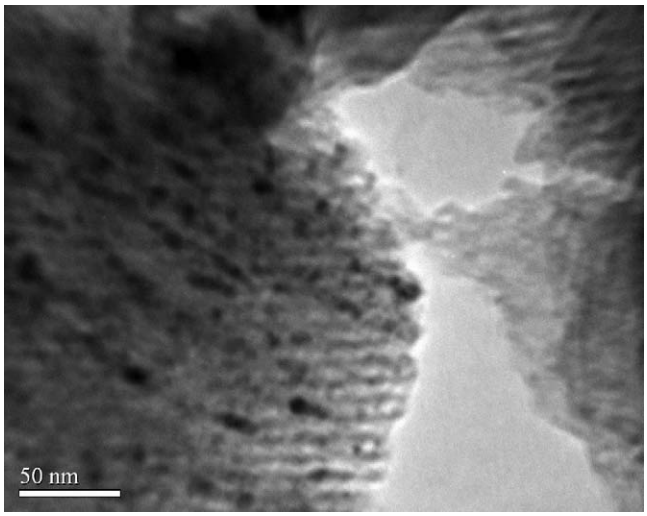

Fig. 4. TEM image of 1%Rh/Ce-SBA-15 catalyst.

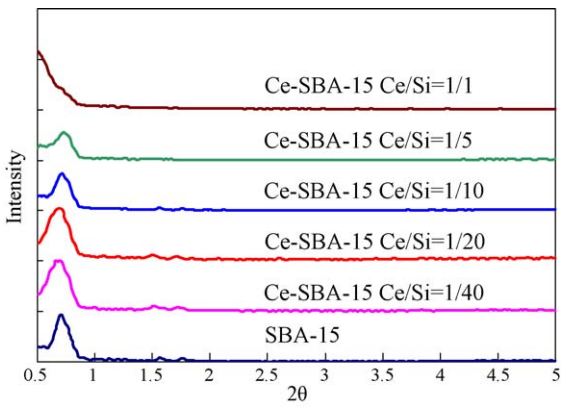

Fig. 5. XRD patterns of 1%Rh/Ce-SBA-15 based catalysts.

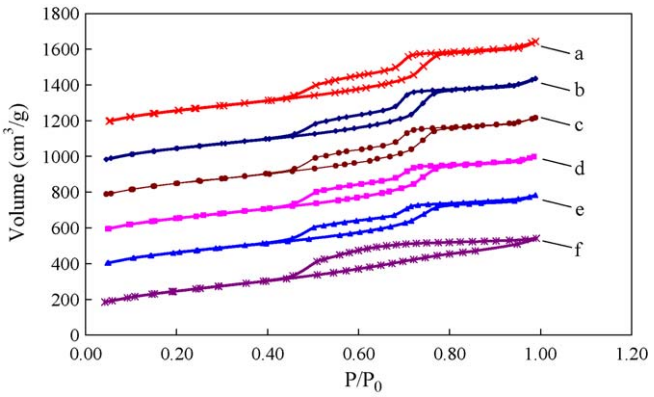

Fig. 6. Nitrogen absorption/desorption isotherms of 1%Rh/Ce-SBA-15 series catalysts under different Ce/Si molar ratio (a) Ce/Si = 1/20, (b) Ce/Si = 1/40, (c) Ce/Si = 0, (d) Ce/Si = 1/10, (e) Ce/Si = 1/5, (f) Ce/Si = 1/1.

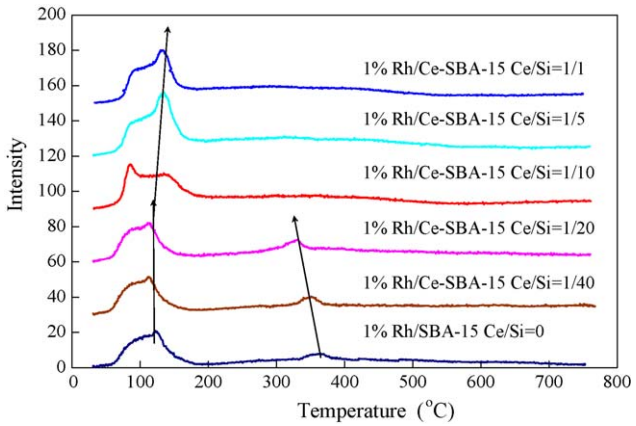

Fig. 7. H_2-TPR profiles of 1%Rh/Ce-SBA-15 series catalysts.

at higher Ce content might have caused the decrease of the mesopore diameter.

3.4. Properties of 1%Rh/Ce-SBA-15 catalysts

Fig. 6 shows the N_2 adsorption/desorption isotherms for a series of 1%Rh/Ce-SBA-15 catalysts, with Ce/Si mole ratio from 0 to 1. When the Ce/Si mole ratio is <1, the adsorption/desorption isotherm of 1%Rh/Ce-SBA-15 catalysts is a typical type IV isotherm with a hysteresis loop, showing that these catalysts possess mesoporous structures [35,46]. When the Ce/Si molar ratio is equal to 1, the type IV isotherm disappears, showing the destruction of ordered mesopores under high Ce content.

As shown in Table 1, the pore diameters of 1%Rh/Ce-SBA-15 increase gradually with the increase of Ce content (from Ce/Si molar ratio = 0 to 1/20), showing the incorporation of Ce into the framework of SBA-15 [42]. The pore diameter then starts to decrease when the Ce/Si molar ratio is subsequently increased from 1/10 to 1/5 due to the formation of cerium oxide nanocrystallites outside the mesopores [35]. However, the pore diameter and specific surface area drop significantly from Ce/Si = 1/5 to Ce/Si = 1/1 due to the destruction of the ordered mesoporous structures at Ce/Si = 1/1 as shown in TEM results (Fig. 3). The N_2 adsorption results are in good agreement with the XRD results, which show the incorporation of Ce (up to Ce/Si = 1/20) into the mesoporous framework of SBA-15. Similar studies have been reported over several mesoporous silica supports incorporated with Mg [29], La [36], Ti [47], U [48], and V [49].

3.5. H_2–TPR profiles of 1%Rh/Ce-SBA-15 series catalysts

Fig. 7 shows H_2–TPR profiles of a series of 1%Rh/Ce-SBA-15 catalysts, whereby Rh species are shown to be reduced over Ce-SBA-15 catalyst supports below 200 °C. In general, the dispersion of active metal oxide, particle sizes, and interaction between active metal and supports can affect the reducibility of active metal [50,51,40,52–54]. Rh oxide species usually has several reduced H_2–TPR peaks due to the presence of different particle sizes of Rh oxide, different Rh valence state, interaction between Rh oxide with support, and the location of Rh oxide species either inside or on the surface of catalysts [50,55–57]. The broad H_2–TPR peak at around 85 °C as observed in our study is due to the reduction of bulk oxide RhO_x species, which is insignificantly affected by the catalyst support, whereas a sharp H_2–TPR peak at around 120 °C is assigned to the bulk oxide Rh_iO_x species, which has been reported to interact with the catalyst support resulting in higher reduction temperature [55].

The factors involved in the preparation of rhodium catalysts, such as calcination temperature and rhodium precursors, are also known to have significant influence on the reducibility of supported Rh species. Calcination temperature has been reported to play an important role in causing a significant increase of the amount of reducible Rh species over Rh/Al_2O_3 calcined at 600 °C than that calcined at 900 °C [57]. Therefore, the calcination temperature at 600 °C has been chosen for this study. Furthermore, using $RhCl_3$ as a precursor, Verykios and co-workers reported that Rh^0, Rh^+, and Rh^{3+} coexisted since residual Cl^- species hindered Rh^{3+} reduction while Rh^{3+} was reduced in the samples using $Rh(NO_3)_3$ as precursors [58]. Therefore, $Rh(NO_3)_3$ has been chosen as the Rh catalyst precursor in this study.

The theoretical value of H_2 consumption required to reduce a series of 1%Rh/Ce-SBA-15 catalysts completely varies from around 22.5 mmol/g to 33.3 mmol/g, while the actual H_2 consumption over these series of catalysts is measured to be from 349.1 umol/g to 412.5 umol/g. This result shows that the actual H_2 consumption required to reduce this series of 1%Rh/Ce-SBA-15 catalysts is only about 1.8% of the total theoretical H_2 consumption, suggesting that only partial mesoporous silica supports could be reduced during the H_2–TPR process [59,60]. Thus H_2 molecules only reduced the Rh oxide species and consumed oxygen species located on the

Table 1
Surface properties of 1%Rh/Ce-SBA-15 based catalysts.

Samples	Pore diameter (DH) (nm)	S_{BET} (m^2/g)	Rh dispersion (%)[a]	Pore volume (cc/g)	Rh content (%)[b]
1%Rh/Ce-SBA-15 (Ce/Si = 0)	7.15	563.2	67.2	0.702	0.95
1%Rh/Ce-SBA-15 (Ce/Si = 1/40)	7.19	579.3	68.5	0.705	0.97
1%Rh/Ce-SBA-15 (Ce/Si = 1/20)	7.25	585.8	69.3	0.708	0.92
1%Rh/Ce-SBA-15 (Ce/Si = 1/10)	7.11	557.2	64.8	0.649	1.16
1%Rh/Ce-SBA-15 (Ce/Si = 1/5)	6.94	530.5	62.9	0.605	0.98
1%Rh/Ce-SBA-15 (Ce/Si = 1/1)	3.56	468.6	58.8	0.519	1.11

[a] From H_2–TPD analysis.
[b] From XPS analysis.

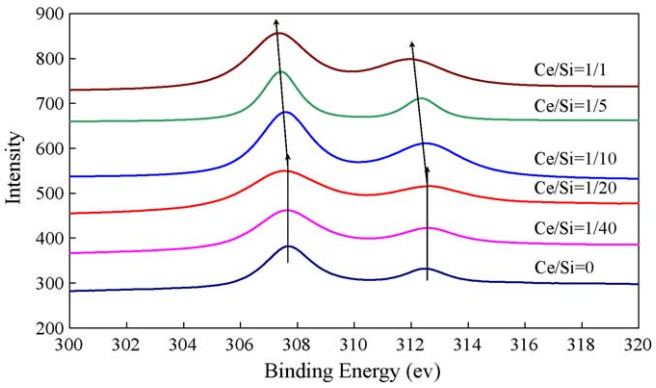

Fig. 8. Rh 3d XP spectra of 1%Rh/Ce-SBA-15 series catalysts at different Ce/Si molar ratio.

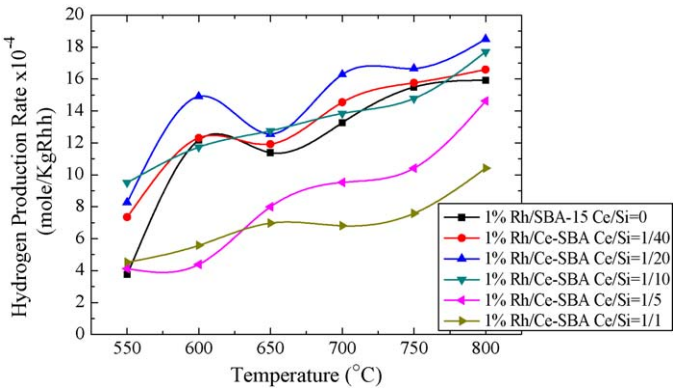

Fig. 9. Effect of catalyst supports on hydrogen production rate over a series of 1%Rh/Ce-SBA-15 based catalysts (molar ratio of C_2H_5OH/CO_2 = 1:1, GHSV = 15594 h^{-1}).

surface of catalyst support [61]. As a result, H_2 consumption peaks can be used to indicate the mobility of surface oxygen over catalyst supports. Similar observation has been reported by some researchers over CeO_2 and Y_2O_3 supports [60–62].

With the increase of Ce/Si molar ratio from 0 to 1/20, the H_2–TPR peaks of partially-reduced supports shift from 370 °C to a lower temperature of around 330 °C, indicating that the surface oxygen species on 1%Rh/Ce-SBA-15 with Ce/Si = 1/20 have higher mobility and activity than those on 1%Rh/Ce-SBA-15 with Ce/Si = 1/40 and 1%Rh/SBA-15. This result suggests that an increase in the amount of incorporated Ce into the mesoporous framework of SBA-15 could promote the mobility and activity of surface oxygen species due to the redox property of Ce ($Ce^{4+} \leftrightarrow Ce^{3+}$) and the formation of oxygen vacancy [63–66].

3.6. XPS analysis of 1%Rh/Ce-SBA-15 based catalysts

Fig. 8 shows Rh 3d XPS spectra of a series of reduced 1%Rh/Ce-SBA-15 based catalysts. Two peaks observed at around 307.2 eV and 312.2 eV are assigned to Rh ($3d_{5/2}$) of Rh^0 and Rh ($3d_{3/2}$) of Rh^0 [58,67]. For pure Rh metal foil, the XPS peaks of Rh($3d_{5/2}$) and Rh($3d_{3/2}$) exhibit at 307.0 eV and 311.8 eV, respectively [58,67,68]. The slightly higher binding energies of the reduced 1%Rh/Ce-SBA-15 than that of the Rh metal foil is attributed to the presence of a small amount of slightly oxidized Rh species on Ce-SBA-15 support [69].

Fig. 8 also shows that the measured Rh ($3d_{5/2}$) and Rh ($3d_{3/2}$) of Rh^0 binding energies at Ce/Si = 0, 1/40, and 1/20 are almost unchangeable; therefore the XPS result is in good agreement with the H_2–TPR results which show that the chemical state of supported Rh species is not affected by the Ce-SBA-15 supports with Ce/Si ratio from 0 to 1/20.

With the increase of Ce content in SBA-15 from Ce/Si = 1/20 to 1/1, Fig. 8 shows that both the binding energies of Rh ($3d_{5/2}$) and Rh ($3d_{3/2}$) of Rh^0 shift to slightly lower binding energies. This phenomenon implies that a higher amount of Rh^0 species have been formed on SBA-15 after reduction, consistent with the H_2–TPR results. When the Ce/Si molar ratio is increased from 1/20 to 1/1, Fig. 7 shows that not only the amount of H_2 consumption increases, as attributed to the reduction of a higher amount of Rh species, but also the H_2–TPR peaks of Rh species shift from 120 °C to 140 °C, as attributed to the decrease of the dispersion of Rh species (Table 1) [50,51,40,53,70].

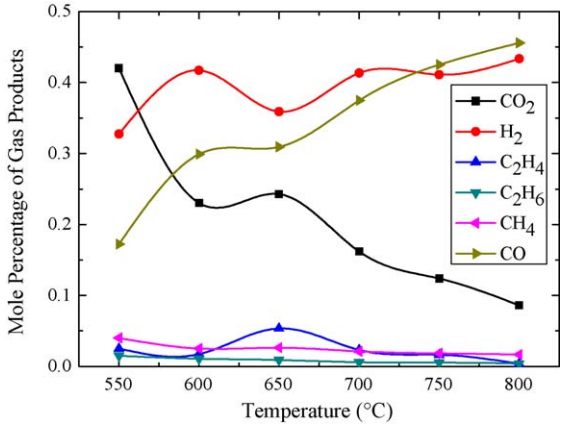

Fig. 10. Mole percentage of gas products over 1%Rh/Ce-SBA-15 (Ce/Si = 1/20, molar ratio of C_2H_5OH/CO_2 = 1:1, GHSV = 15594 h^{-1}).

3.7. Activity test

Fig. 9 shows the hydrogen production rate for CO_2 reforming of ethanol over a series of 1%Rh/Ce-SBA-15 based catalysts. An increase of reaction temperature generally yields higher hydrogen production rate over these catalysts because CO_2 reforming of ethanol is an endothermic reaction which causes higher yield of H_2 at higher temperature. Among these catalysts, 1%Rh/Ce-SBA-15

Table 2
Conversion of CO_2 over 1%Rh/Ce-SBA-15 series catalysts.

Sample	Conversion of CO_2					
	550 °C	600 °C	650 °C	700 °C	750 °C	800 °C
1%Rh/Ce-SBA-15 Ce/Si = 0	0.14	0.53	0.48	0.62	0.65	0.71
1%Rh/Ce-SBA-15 Ce/Si = 1/40	0.19	0.52	0.5	0.64	0.69	0.75
1%Rh/Ce-SBA-15 Ce/Si = 1/20	0.2	0.57	0.53	0.68	0.76	0.83
1%Rh/Ce-SBA-15 Ce/Si = 1/10	0.23	0.49	0.54	0.62	0.64	0.78
1%Rh/Ce-SBA-15 Ce/Si = 1/5	0.15	0.24	0.35	0.44	0.48	0.59
1%Rh/Ce-SBA-15 Ce/Si = 1/1	0.15	0.28	0.31	0.3	0.38	0.46

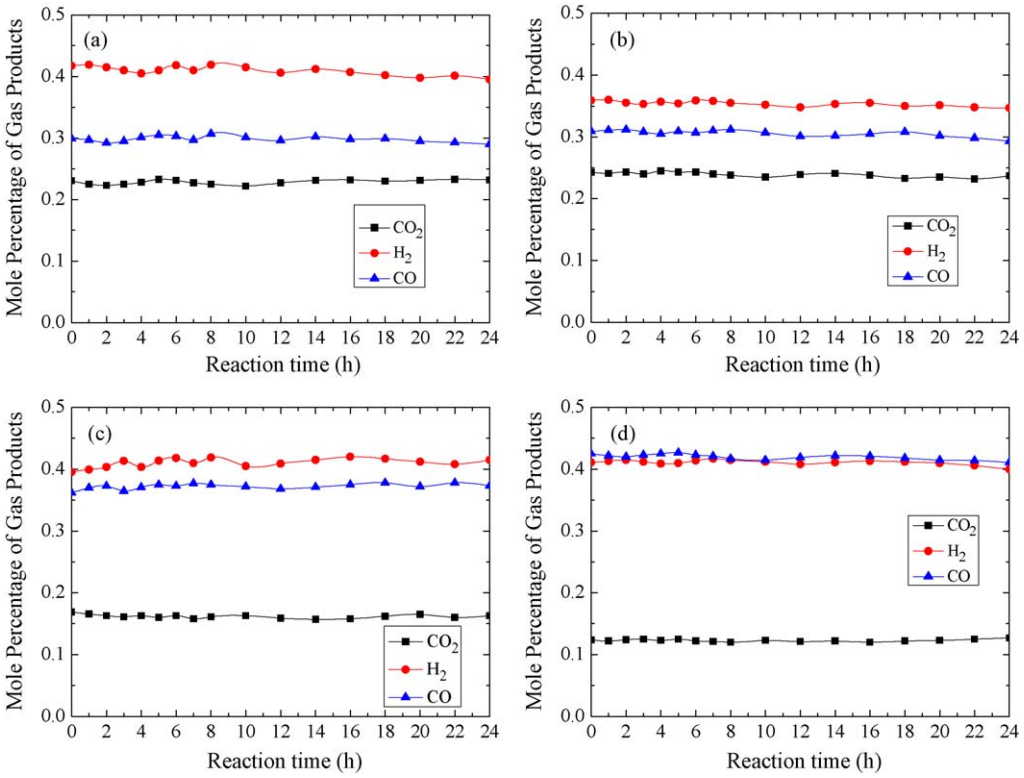

Fig. 11. Stability study of 1%Rh/Ce-SBA-15 Ce/Si = 1/20 (molar ratio of C_2H_5OH/CO_2 = 1:1, GHSV = 15594 h^{-1}), mole percentage of gas products during 24 h running at (a) 600 °C, (b) 650 °C, (c) 700 °C and (d) 750 °C.

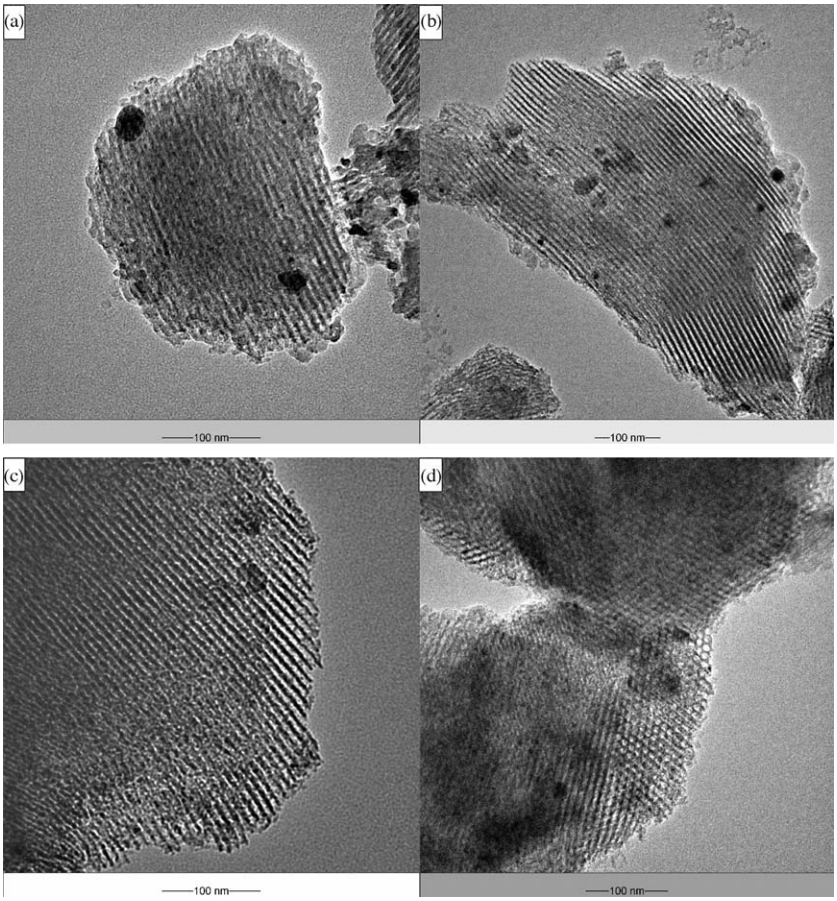

Fig. 12. TEM images of 1%Rh/Ce-SBA-15 Ce/Si = 1/20 after 24 h running (molar ratio of C_2H_5OH/CO_2 = 1:1, GHSV = 15594 h^{-1}) at different reaction temperatures, (a) 600 °C, (b) 650 °C, (c) 700 °C, and (d) 750 °C.

(Ce/Si = 1/20) catalyst is observed to give the highest H_2 production rate at 550–800 °C. It was reported that the enhancement of activity was due to the higher Rh dispersion in some reactions such as N_2O decomposition and partial oxidation of methane [41,71]. Table 1 shows that the Rh dispersion over Rh/Ce-SBA-15 catalysts (with Ce/Si from 0 to 1/20) is different from that of Rh/Ce-SBA-15 catalysts (with Ce/Si from 1/10 to 1/1), indicating that the decrease of Rh dispersion is the factor causing the decrease of the catalytic performance of Rh/Ce-SBA-15 catalysts with Ce/Si molar ratio from 1/10 to 1/1 for CO_2 reforming of ethanol. Based on these results, the mobility of surface oxygen species and Rh dispersion over catalyst support are both found to play important roles in achieving high catalytic performance [62,72–74].

The increase of the catalytic activity of 1%Rh/Ce-SBA-15, with Ce/Si molar ratio increasing from 0 to 1/20 for CO_2 reforming of ethanol is attributed to the increase of the amount of Ce incorporated into the SBA-15 framework, which enhances the mobility of surface oxygen species due to the redox property of Ce ($Ce^{4+} \leftrightarrow Ce^{3+}$) and the formation of oxygen vacancy [63–65]. When the Ce/Si molar ratio is further increased from 1/20 to 1/1, the catalytic activity of 1%Rh/Ce-SBA-15 catalyst decreases due to the decrease of Rh dispersion which causes the decrease of catalytic activity [41,71]. As a result, the optimal Ce/Si molar ratio for the highest hydrogen production rate is 1/20.

Fig. 10 shows the mole percentage distribution of gas products produced from CO_2 reforming of ethanol over 1%Rh/Ce-SBA-15 (Ce/Si = 1/20) catalyst. The amount of minor products (CH_4, C_2H_4, and C_2H_6) is close to zero, indicating that main reaction of CO_2 reforming of ethanol (Eq. (1)) is dominant at the temperature range of 550–800 °C. With the increase of reaction temperature from 600 °C to 650 °C, the hydrogen production rate drops significantly because the dehydration reaction, which is a side reaction, is promoted at this temperature and thus increases the mole percentage of C_2H_4 (Figs. 9 and 10). Since this dehydration reaction does not produce hydrogen (Eq. (3)), hydrogen production rate decreases at higher temperature [14,15]. Similar catalytic behavior has also been reported over the decomposition of ethanol (Eq. (7)) by Szchenyi and Solymosi [15]. It is worth to note that at the reaction temperature higher than 650 °C, the molar ratio of H_2/CO is between 0.9 and 1.2, which is suitable for the production of liquid hydrocarbons or oxygenated hydrocarbons [11,12]. Furthermore, Table 2 shows that the CO_2 conversion generally increases with the increase of reaction temperature and the 1%Rh/Ce-SBA-15 (Ce/Si = 1/20) catalyst has the highest conversion of CO_2 (about 75%) at around 700–750 °C during CO_2 reforming of ethanol (with CO_2/ethanol molar ratio = 1).

3.8. Stability test

Fig. 11 shows the catalytic stability of the 1%Rh/Ce-SBA-15 (Ce/Si = 1/20) catalyst during the CO_2 reforming of ethanol for 24 h. The mole percentage of gas products (such as H_2, CO, C_2H_4, C_2H_6 and CH_4) is almost constant on stream at 600 °C, 650 °C, 700 °C and 750 °C. The 1%Rh/Ce-SBA-15 (Ce/Si = 1/20) catalyst has the highest hydrogen production yield at 700 °C and 750 °C. Furthermore, as the reaction temperature increases, CO_2 conversion increases and H_2/CO molar ratio approaches to about 1.

Fig. 12 displays the TEM images of the 1%Rh/Ce-SBA-15 (Ce/Si = 1/20) used catalyst. It can be seen that the hexagonal mesopores of SBA-15 of the used catalyst are still kept intact, even after these catalysts have been used in CO_2–ethanol reforming reaction for 24 h at 600 °C, 650 °C, 700 °C and 750 °C. This result shows that the 1%Rh/Ce-SBA-15 (Ce/Si = 1/20) catalyst is a potential commercial catalyst for CO_2 reforming with ethanol to produce syngas and hydrogen.

4. Conclusions

CO_2 reforming of ethanol has been used successfully to produce syngas or hydrogen over Rh/Ce-SBA-15 catalysts. The mobility of surface oxygen species and Rh dispersion over Ce/SBA-15 catalyst support are both found to play important roles in achieving high catalytic performance. The increase of catalytic activity over 1%Rh/Ce-SBA-15 from Ce/Si = 0 to Ce/Si = 1/20 in CO_2 reforming of ethanol is due to the increase of the amount of incorporated Ce into SBA-15 crystalline lattice, which promotes the mobility of surface oxygen species. The optimal Ce/Si molar ratio for the highest hydrogen production rate is 1/20. The hexagonal mesopores of Ce/SBA-15 remains intact during prolonged reaction even up to 750 °C. Therefore, the 1%Rh/Ce-SBA-15 (Ce/Si = 1/20) catalyst is shown to be a potential commercial catalyst for CO_2 reforming with ethanol to produce syngas (with H_2/CO ratio around 1) or hydrogen.

Acknowledgements

The authors acknowledge the support from NUS (R-279-000-232-112) and ASTAR (SERC-092-138-0022) funding.

References

[1] R.A. Kerr, Science 312 (2006) 1854.
[2] T.R. Knutson, R.E. Tuleya, Y. Kurihara, Science 279 (1998) 1018.
[3] R.A. Feely, R. Wanninkhof, T. Takahashi, P. Tans, Nature 398 (1999) 597.
[4] U. Riebesell, I. Zondervan, B. Rost, P.D. Tortell, R.E. Zeebe, F.M.M. Morel, Nature 407 (2000) 364.
[5] S. Barker, H. Elderfield, Science 297 (2002) 833.
[6] I.P. Montanez, N.J. Tabor, D. Niemeier, W.A. DiMichele, T.D. Frank, C.R. Fielding, J.L. Isbell, L.P. Biegenheirer, M.C. Rygel, Science 315 (2007) 87.
[7] M.A. Goula, S.K. Kontou, P.E. Tsiakaras, Appl. Catal. B 49 (2004) 135.
[8] S. Velua, K. Suzukia, M. Vijayaraj, S. Barmanb, C.S. Gopinathb, Appl. Catal. B 55 (2005) 287.
[9] G.A. Deluga, J.R. Salge, L.D. Schmidt, X.E. Verykios, Science 303 (2004) 993.
[10] K.J. Puolakka, A.O.I. Krause, Catal. Lett. 116 (2007) 87.
[11] E. Adolfo, C. Luna, M.E. Iriarte, Appl. Catal. A 343 (2008) 10.
[12] X.L. Zhu, P.P. Huo, Y.P. Zhang, D.G. Cheng, C.J. Liu, Appl. Catal. B 81 (2008) 132.
[13] J.D.A. Bellido, E.Y. Tanable, E.M. Assaf, Appl. Catal. B 90 (2009) 485.
[14] W.L. Li, H. Wang, Z.Y. Ren, G. Wang, J.B. Bai, Appl. Catal. B 84 (2008) 433.
[15] A. Szchenyi, F. Solymosi, J. Phys. Chem. C 111 (2007) 9509.
[16] M. Cimenti, J.M. Hill, J. Power Sources 186 (2009) 377.
[17] V. Fierro, V. Klouz, O. Akdim, C. Mirodatos, Catal. Today 75 (2002) 141.
[18] J.P. Breen, R. Burch, H.M. Coleman, Appl. Catal. B 39 (2002) 65.
[19] Y.G. Chen, K. Tomishige, K. Yokoyama, K. Fujimoto, J. Catal. 184 (1999) 479.
[20] M.A. Goula, A.A. Lemonidou, A.M. Efstathiou, J. Catal. 161 (1996) 626.
[21] S. Wang, G.Q.M. Lu, Appl. Catal. B 16 (1998) 269.
[22] S. Tang, L. Ji, J. Lin, H.C. Zeng, K.L. Tan, K. Li, J. Catal. 194 (2000) 424.
[23] J.Z. Luo, Z.L. Yu, C.F. Ng, C.T. Au, J. Catal. 194 (2000) 198.
[24] G. Wang, H. Wang, Z. Tang, W. Li, J. Bai, Appl. Catal. B (2008), doi:10.1016/j.apcatb.2008.09.008.
[25] F. Aupretre, C. Descorme, D. Duprez, D. Casanave, D. Uzio, J. Catal. 233 (2005) 464.
[26] J.F. Munera, S. Irusta, L.M. Cornaglia, E.A. Lombardo, D.V. Cesar, M. Schmal, J. Catal. 245 (2007) 25.
[27] J.H. Bitter, K. Seshan, J.A. Lercher, J. Catal. 176 (1998) 93.
[28] M. Maestri, D.G. Vlachos, A. Beratta, G. Groppi, E. Tronconi, J. Catal. 259 (2008) 211.
[29] D.T. On, D. Desplantier-Giscard, C. Danumah, S. Kaliaguine, Appl. Catal. A 222 (2001) 299.
[30] A.J. Vizcaino, A. Carrero, J.A. Calles, Catal. Today (2009), doi:10.1016/j.cattod.2008.11.020.
[31] H. Liu, H. Wang, J. Shen, Y. Shun, Z. Liu, Appl. Catal. A 337 (2008) 138.
[32] P. Shah, V. Ramaswamy, Microporous Mesoporous Mater. 114 (2008) 270.
[33] D.W. Lee, C.Y. Yu, K.H. Lee, J. Phys. Chem. C 112 (2008) 5136.
[34] A. Beck, A. Horvath, Gy. Stefler, R. Katona, O. Geszti, Gy. Tolnai, L.F. Liotta, L. Guczi, Catal. Today 139 (2008) 180.
[35] M.N. Timofeeva, S.H. Jhung, Y.K. Hwang, D.K. Kim, V.N. Panchenko, M.S. Melgunov, Yu.A. Chesalov, J.S. Chang, Appl. Catal. A 317 (2007) 1.
[36] J.A. Calles, A. Carrero, A.J. Vizcaino, Microporous Mesoporous Mater. 119 (2009) 200.
[37] C. Loschen, A. Migani, S. Bromley, T.F. Illas, K.M. Neyman, Phys. Chem. Chem. Phys. 10 (2008) 5730.
[38] D. Zhao, J. Feng, Q. Huo, N. Melosh, G.H. Fredrickson, B.F. Chmelka, G.D. Stucky, Science 279 (1998) 23.
[39] S.W. Song, K. Hidajat, S. Kawi, Langmuir 21 (2005) 9568.
[40] C. Carrara, A. Roa, L. Cornaglia, E.A. Lombardo, C. Mateos-Pedrero, P. Ruiz, Catal. Today 133–135 (2008) 344.
[41] J. Du, W. Kuang, H. Xu, W. Shen, D. Zhao, Appl. Catal. B 84 (2008) 490.

[42] Z. Mu, J.J. Li, H. Tian, Z.P. Hao, S.Z. Qiao, Mater. Res. Bull. 43 (2008) 2599.
[43] X. Xu, J. Li, Z. Hao, W. Zhao, C. Hu, Mater. Res. Bull. 41 (2006) 406.
[44] Q. Dai, X. Wang, G. Chen, Y. Zheng, G. Lu, Microporous Mesoporous Mater. 100 (2007) 268.
[45] A. Carrero, J.A. Calles, A.J. Vizcaino, Appl. Catal. A 327 (2007) 82.
[46] D. Zhao, Q. Huo, J. Feng, B.F. Chmelka, G.D. Stucky, J. Am. Chem. Soc. 120 (1998) 6024.
[47] G.A. Eimer, S.G. Casuscelli, G.E. Ghione, M.E. Crivello, E.R. Herrero, Appl. Catal. A 298 (2006) 232.
[48] D. Kumar, P.U. Sastry, D. Sen, N.M. Gupta, Microporous Mesoporous Mater. 89 (2006) 132.
[49] Y. Segura, P. Cool, P. Kustrowski, L. Chmielarz, R. Dziembaj, E.F. Vansant, J. Phys. Chem. B 109 (2005) 12071.
[50] J.A. Wang, T. Lopez, X. Bokhimi, O. Novaro, J. Mol. Catal. A 239 (2005) 249.
[51] J. Peng, S. Wang, Appl. Catal. B 73 (2007) 282.
[52] Z.J. Wang, Y. Liu, P. Shi, C.J. Liu, Y. Liu, Appl. Catal. B 90 (2009) 570.
[53] M.M. Hossain, Chem. Eng. J. 123 (2006) 15.
[54] L. Jiao, J.R. Regalbuto, J. Catal. 260 (2008) 342.
[55] C.P. Hwang, C.T. Yeh, Q. Zhu, Catal. Today 51 (1999) 93.
[56] J.A. Sullivan, J. Cunningham, Appl. Catal. B 15 (1998) 275.
[57] W.Z. Weng, X.Q. Pei, J.M. Li, C.R. Luo, Y. Liu, H.Q. Lin, C.J. Huang, H.L. Wan, Catal. Today 117 (2006) 53.
[58] D.I. Kondarides, X.E. Verykios, J. Catal. 174 (1998) 52.
[59] F.B. Passos, E.R. Oliveria, L.V. Mattos, F.B. Noronhe, Catal. Lett. 110 (2006) 261.
[60] G.B. Sun, K. Hidajat, X.S. Wu, S. Kawi, Appl. Catal. B 81 (2008) 303.
[61] S.S. Lin, C.L. Chen, D.J. Chang, C.C. Chen, Water Res. 36 (2002) 3009.
[62] E. Mamontov, T. Egami, R. Brezny, M. Koranne, S. Tyagi, J. Phys. Chem. B 104 (2000) 11110.
[63] C.T. Campbell, C.H.F. Peden, Science 309 (2005) 713.
[64] F. Esch, S. Fabris, L. Zhou, T. Montini, C. Africh, P. Fornasiero, G. Comelli, R. Rosei, Science 309 (2005) 752.
[65] C.H. Liang, Z.Q. Ma, H.Y. Lin, J. Mater. Chem. 19 (2009) 1417.
[66] A. Igarashi, N. Ichikawa, S. Sato, R. Takahashi, T. Sodesawa, Appl. Catal. A 300 (2006) 50.
[67] A. Gayen, K.R. Priolkar, R. Sarode, V. Jayaram, M.S. Hegde, G.N. Subbabba, S. Emura, Chem. Mater. 16 (2004) 2317.
[68] K. Polychronopoulou, J.L.G. Fierro, A.M. Efstathiou, J. Catal. 228 (2004) 417.
[69] R. Wang, H. Xu, X. Liu, Q. Ge, W. Li, Appl. Catal. A 305 (2006) 204.
[70] N.W. Hurst, S.J. Gentry, A. Jones, Catal. Rev. Sci. Eng. 24 (2) (1982) 233.
[71] S. Eriksson, S. Rojas, M. Boutonnet, J.L.G. Fierro, Appl. Catal. A 326 (2007) 8.
[72] J. Guzman, S. Carrettin, A. Corma, J. Am. Chem. Soc. 127 (2005) 3286.
[73] V. Aguilar-Guerrero, B.C. Gates, J. Catal. 260 (2008) 351.
[74] J. Guzman, S. Carrettin, J.C.F. Gonzalez, Y. Hao, B.C. Gates, A. Corma, Angew. Chem. Int. Ed. 44 (2005) 4778.